Patterning Multilayers of Molecules via Self-Organization

Wei Lu* and David Salac

Department of Mechanical Engineering, University of Michigan, Ann Arbor, Michigan 48109, USA

(Received 19 October 2004; published 13 April 2005)

The electric dipole interaction among adsorbate molecules may cause them to form regular nanopatterns. In a multilayer system, the self-organization of each layer is also influenced by the underlying layers. This Letter develops a phase field model to simulate the molecular patterning process. The study reveals self-alignment, scaling down of size, and the effect of guided self-assembly with embedded electrodes.

DOI: 10.1103/PhysRevLett.94.146103 PACS numbers: 68.43.Hn, 68.35.Md

An adsorbate molecule usually carries an electric dipole. Even if the molecules are nonpolar, the act of binding onto a substrate breaks the symmetry and causes the formation of dipoles. A molecule can be engineered to carry a large electric dipole moment by incorporating a polar group [1]. Characterized by the $1/\text{distance}^3$ variation in energy, dipole type interaction can be induced by electric, magnetic, or elastic fields. Studies have shown that dipole interactions give rise to domain patterns. Examples include Langmuir films at the air-water interface [2], ferrofluids in magnetic fields [3], organic molecules on metal surface [4], and surface stress induced self-organization on elastic substrates [5]. Despite the difference of these systems, similar phenomenology and mechanism can be identified. The adsorbed molecules are mobile [6]. Domains coarsen to reduce the domain boundary and refine to reduce the dipole interaction energy. The competition leads to equilibrium patterns, whose sizes range from the nanometer to centimeter scale. This mechanism may be used to make two-dimensional nanostructures. Specifically, molecule monolayers composed of electric dipoles can be manipulated with an electric field induced by an antiferromagnetic tip, a ceiling above the layer, or an electrode array in the substrate [7–9].

Charge interactions have been utilized to construct functional multilayer systems by the approach of electrostatic self-assembly (ESA) [10]. ESA processing involves dipping a chosen substrate into alternate aqueous solutions containing anionic and cationic molecules or nanoparticles, such as complexes of polymers, metal and oxide nanoclusters, or proteins. This leads to alternating layers of polyanion and polycation monolayers. Design of the precursor molecules and control of the order of the multiple molecular layers allow control over macroscopic electrical, optical, mechanical, and other properties. While applications such as nanofiltration and photovoltaic devices [10] have been demonstrated, the ESA process is limited to simple, laminar multilayer systems, with little or no lateral variation in the monolayer. We show that for molecules carrying electric dipoles, dipole interaction can induce self-assembled patterns within each layer in a multilayer system. The capability is desired for making complex structures, especially the formation of nanointerfaces and three-dimensional nanocomposites. We also reveal self-alignment between layers, reduction of feature sizes, and guided self-assembly by layer-layer interaction and embedded electrodes.

Consider a multilayer of molecules adsorbed onto a substrate, as shown in Fig. 1. The first layer contacts the substrate, and the nth layer is the top layer. Each layer has a thickness of h_m ($m = 1$ to n) and the total thickness is h_f. The space above the top layer can be air or a dielectric fluid. An array of electrodes is embedded at a distance of h_s from the substrate surface. Each layer comprises two molecular species carrying different dipole moments. We describe the dipole pattern formation in each layer by a phase field approach [11,12]. For the nth layer, let concentration C_n be the fraction of surface sites occupied by one of the two species, and regard it as a time-dependent, spatially continuous function, $C_n(x_1, x_2, t)$. The free energy of the top layer is given by

$$G = \int_A \left[g(C_n) + \beta |\nabla C_n|^2 + \frac{1}{2}\left(\frac{p_n}{h_n}\right)(\Delta\phi_n)_s \right] dA + \int_A \left(\frac{p_n}{h_n}\right)(\Delta\phi_n)_e dA. \quad (1)$$

The first integral is the "self-energy" of the layer. The $g(C_n)$ term represents the chemical energy. We also lump any interface energy between the nth layer and its underlying layer into this term. To describe phase separation, we

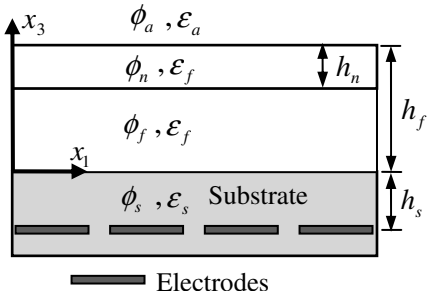

FIG. 1. Schematic of a multilayer system. The substrate occupies the half-space $x_3 < 0$ bounded by the x_1-x_2 plane.

may prescribe $g(C_n)$ by any function with two wells. We assume a regular solution, and the energy per unit area is given by $g(C_n) = \Lambda k_B T[C_n \ln C_n + (1 - C_n)\ln(1 - C_n) + \Omega C_n(1 - C_n)]$. Here Λ is the number of surface sites per unit area, k_B the Boltzmann constant, T the absolute temperature, and Ω a dimensionless parameter measuring the bonding strength relative to the thermal energy. When $\Omega > 2$, the function $g(C_n)$ has double wells and the binary mixture separates into two phases. The second term is the phase boundary energy within the layer, and β is a material constant. These two terms are typical in the Cahn-Hilliard equation [11]. The third term is the dipole assembly energy, i.e., the work to bring the dipole charges from infinity to the current configuration. Here p_n is the dipole density per unit area. The quantity $(\Delta\phi_n)_s$ is the potential jump across the layer thickness due to the dipole interaction within the layer. Note that $(\Delta\phi_n)_s$, and thus the assembly energy, is affected by the environment including the dielectric properties of the underlying layers and the substrate. The calculation of $(\Delta\phi_n)_s$ will be given later. We interpolate p_n linearly by the dipole densities of the two species, giving $p_n = \xi_n + \eta_n C_n$, where ξ_n and η_n are material constants.

The second integral in Eq. (1) is the interactive energy of the top layer with the underlying layers and the substrate. The dipoles in other layers and the applied field by the electrodes cause a potential difference, $(\Delta\phi_n)_e$, between the $x_3 = h_f$ and $x_3 = h_f - h_n$ surfaces in the dielectric media. The term $(p_n/h_n)(\Delta\phi_n)_e$ represents the energy of the top layer due to $(\Delta\phi_n)_e$. The factor of $1/2$ marks the difference in the expressions of the dipole assembly energy, and the energy of dipoles in a given electric field.

The molecules in the top layer diffuse to reduce the energy given in Eq. (1). We assume that the buried layers will not diffuse. This assumption is motivated by the observation that molecules at the surface have much higher mobility than those inside. The buried layers diffuse so slowly that they can be considered immobile. Following a procedure similar to that in Ref. [12], we obtain

$$\frac{\partial C_n}{\partial t} = \frac{M}{\Lambda^2}\nabla^2\left[\frac{\partial g}{\partial C_n} - 2\beta\nabla^2 C_n + \eta_n(\Delta\phi_n)_s/h_n + \eta_n(\Delta\phi_n)_e/h_n\right], \quad (2)$$

where M is the mobility of molecules. The last two terms in the large bracket couple the evolution of the molecules to the electrostatic field. The calculation starts from the first layer. At a given time, the molecule distribution C_1 is known. The electrostatic field is determined by solving the boundary value problems. The resulting $(\Delta\phi_1)_s$ and $(\Delta\phi_1)_e$ enter the right-hand side of Eq. (2). Repeat the procedure for many time steps until the prescribed time. Then start the calculation for the second layer, and so on. When considering the nth layer, the molecule distributions of C_m ($m = 1$ to $n - 1$) are known from previous calculations. As will be evident, $(\Delta\phi_n)_s$ depends on C_n and $(\Delta\phi_n)_e$ depends on C_m ($m = 1$ to $n - 1$).

Figure 1 illustrates the calculation of $(\Delta\phi_n)_s$. The nth layer has an area dipole density of p_n. This dipole distribution is equivalent to a surface charge density of p_n/h_n at $x_3 = h_f$ and $-p_n/h_n$ at $x_3 = h_f - h_n$. The electric potential fields in the four regions, i.e., air, the nth layer, the underlying layers, and the substrate, are denoted by ϕ_a, ϕ_n, ϕ_f, and ϕ_s. For simplicity, we assume that all the adsorbate layers have the same permittivity ε_f. The permittivities of the air and the substrate are ε_a and ε_s. The electric potential satisfies the Laplace equation and is continuous across the boundary. The surface charge density causes a jump of electric displacement according to Gauss's law. Take ϕ_n as an example. In the layer $\nabla^2\phi_n = 0$. At the boundary of ϕ_n and ϕ_f, i.e., $x_3 = h_f - h_n$, we have $\phi_n = \phi_f$ and $-\varepsilon_f(\partial\phi_n/\partial x_3) + \varepsilon_f(\partial\phi_f/\partial x_3) = -p_n/h_n$. Similar relations can be written for other regions and boundaries. Note that without applied voltage we have $\phi_s(x_3 = -h_s) = 0$. The set of equations can be solved analytically with Fourier transform to x_1 and x_2. The solution is $(\Delta\hat{\phi}_n)_s/h_n = -k(\eta_n\varepsilon_a/\varepsilon_f^2)W_k\hat{C}_n$, where the "hat" indicates Fourier transform, $k = \sqrt{k_1^2 + k_2^2}$, and k_1, k_2 are the coordinates in Fourier space. In the expression we have $W_k = [\sinh(kh_f)\sinh(kh_s) + \cosh(kh_f) \times \cosh(kh_s)(\varepsilon_s/\varepsilon_f)]/D$ and $D = \sinh(kh_f)[\sinh(kh_s) + \cosh(kh_s)(\varepsilon_a\varepsilon_s/\varepsilon_f^2)] + \cosh(kh_f)[\sinh(kh_s)(\varepsilon_a/\varepsilon_f) + \cosh(kh_s)(\varepsilon_s/\varepsilon_f)]$. A similar approach solves the electrostatic field induced by the total $n - 1$ layers of dipoles and the prescribed potential of $\phi_s(x_1, x_2, -h_s) = U(x_1, x_2)$. We obtain that $(\Delta\hat{\phi}_n)_e/h_n = -k(\eta_n\varepsilon_a/\varepsilon_f^2)R_k$, where $R_k = (1/D)[\hat{U}\varepsilon_s/\eta_n + \sum_{m=1}^{n-1}(\eta_m\hat{C}_m/\eta_n)[\sinh(kz_m) \times \sinh(kh_s) + \cosh(kz_m)\cosh(kh_s)(\varepsilon_s/\varepsilon_f)]$, and $z_m = \sum_{j=1}^{m} h_j$ is the distance between the upper surface of the mth layer and the substrate.

A comparison of the first two terms in Eq. (2) defines a length $b = \sqrt{\beta/\Lambda k_B T}$. In the Cahn-Hilliard model, this length scales the phase boundary thickness. A time scale is defined by $\tau = \beta/[M(k_B T)^2]$. Normalize the coordinates by b and the time by τ. A dimensionless number

$$s_n = \frac{\varepsilon_a \eta_n^2}{\varepsilon_f^2\sqrt{\beta\Lambda k_B T}} \quad (3)$$

appears in the normalized equation. This number represents the strength of dipole interactions relative to the phase boundary energy and affects the equilibrium phase size. The diffusion equation (2) in Fourier space is given by

$$\frac{\partial\hat{C}_n}{\partial t} = -k^2\hat{P}_n - 2k^4\hat{C}_n + k^3 s_n W_k\hat{C}_n + k^3 s_n R_k, \quad (4)$$

where $\hat{P}_n(k_1, k_2)$ is the Fourier transform of $P_n(x_1, x_2) = \ln[C_n/(1 - C_n)] + \Omega(1 - 2C_n)$. Equation (4) can be solved efficiently with the semi-implicit method [12].

Two limiting situations give insight into the problem. First consider a monolayer, i.e., $n = 1$ and $h_f = h_n$. The jump of the electric potential across the monolayer is often referred to as the contact potential, and can be measured experimentally by the Kelvin method [1]. For instance, the typical value for alkanethiols on gold can vary between -0.75 V to 0.6 V depending on the specific structure. The contact potential $\Delta\phi$ relates to the monolayer dipole density p by $\Delta\phi = p/\varepsilon_f$. The expression for W_k reduces to $1/[1 + (\varepsilon_a/\varepsilon_s)\tanh(kh_s)]$ since the layer thickness is much smaller than the phase size. We estimate the equilibrium size by a linear perturbation analysis, considering only one Fourier component of wavelength λ. The equilibrium wavelength λ_{eq} is obtained by minimizing Eq. (1) as a function of λ. This estimation is more accurate when the equilibrium concentration profile is closer to a sinusoidal or cosinusoidal wave. When the profile is closer to a square wave, more Fourier components are needed for a precise computation. Assume $U = 0$ since our interest is the intrinsic length scale. The analysis shows that $\lambda_{\text{eq}}^0 = 8\pi b/s_1$ when $h_s = 0$, and $\lambda_{\text{eq}}^\infty = 8\pi(1 + \varepsilon_a/\varepsilon_s)b/s_1$ when $h_s \to \infty$. The expression is more complicated when h_s is in the midrange. The two situations, $h_s = 0$ and $h_s \to \infty$, correspond to a monolayer on a metal substrate and on a semi-infinite dielectric substrate, respectively. The phase size can be tuned through the dielectric properties of the air and the substrate since $\lambda_{\text{eq}}^\infty$ increases with $\varepsilon_a/\varepsilon_s$. Note that λ_{eq}^0 is smaller than $\lambda_{\text{eq}}^\infty$, indicating that the dipole interaction is stronger on a metal surface. The expression of λ_{eq}^0 can also be obtained consistently by letting $\varepsilon_s \to \infty$ in $\lambda_{\text{eq}}^\infty$. Equation (3) suggests that larger dipole density, lower adsorbate permittivity, and lower phase boundary energy lead to a smaller phase size. Specifically, doubling the dipole density reduces the size to 1/4 of the original size.

The other limiting situation is many layers, i.e., $h_f \to \infty$. The expression for W_k reduces to $1/(1 + \varepsilon_a/\varepsilon_f)$. Neglecting $(\Delta\phi_n)_e$, we obtain $\lambda_{\text{eq}} = 8\pi(1 + \varepsilon_a/\varepsilon_f)b/s_n$ for the top layer. Note that the substrate permittivity is irrelevant. The analysis shows that h_f can be considered large when $h_f > \lambda_{\text{eq}}$. The difference between λ_{eq} and $\lambda_{\text{eq}}^\infty$ (or λ_{eq}^0) suggests a phase size transition during the layer-by-layer growth. Obviously, the size can be designed to vary significantly between layers with molecules carrying different dipoles. Gradual phase size refining over growth can be achieved. The self-assembly process is guided by $(\Delta\phi_n)_e$. The contribution of U can be neglected when h_f is large since D increases exponentially. A simple expression of $R_k = \hat{C}\eta/[\eta_n(1 + \varepsilon_a/\varepsilon_f)]$ exists when the underlying layers have the same $\eta_m = \eta$ and $\hat{C}_m = \hat{C}$. Comparison between R_k and W_k shows that $(\Delta\phi_n)_e$ and $(\Delta\phi_n)_s$ have the same order. This strong layer-layer interaction leads to self-alignment of patterns. To explain the idea, consider a representative Fourier component with wavelength λ. Assume $C_m = q_1 \sin(2\pi x_1/\lambda)$ for the underlying layers and $C_n = q_2 \sin[2\pi(x_1 + a)/\lambda]$ for the top layer, where q_1, q_2 are two positive amplitudes and a ($0 \le a < \lambda$) is the pattern shift. The average energy per unit area, $\bar{g}$, can be calculated with Eq. (1), which gives $\bar{g} = g_1 - q_1 q_2 \cos(2\pi a/\lambda)\pi\eta_n\eta\varepsilon_a/[2\varepsilon_f(\varepsilon_f + \varepsilon_a)]$, where g_1 is independent of a. The energy is minimized when $a = 0$; i.e., the top layer pattern aligns with that of the underlying layers. When h_f is large, only a total thickness of λ_{eq} beneath layers is significant to the top layer pattern. It can be expected that this self-alignment mechanism will facilitate the pattern formation of subsequent layers and increase uniformity.

An arbitrary number of layers can be considered by numerical simulations. This Letter focuses on two layers. The guiding effect of the electrodes and the underlying layer is of particular interest. Simulations are carried out with $256b \times 256b$ grids and periodic boundary conditions. The initial conditions are random. That is, the concentration has an average of $\bar{C}_n$ in the nth layer. The initial concentrations at the grid points fluctuate randomly within 0.001 from the average. The parameters used in all simulations are $\Omega = 2.2$, $\varepsilon_a/\varepsilon_s = \varepsilon_f/\varepsilon_s = 1$, $h_s/b = 10$, $h_1/b = h_2/b = 0.5$. First consider the situation without external field. Figure 2 shows selected results for $U = 0$ and $s_1 = s_2 = 4$, darker color for higher concentration. A monolayer self-assembles into a triangular of dots when the average concentration is $\bar{C}_1 = 0.3$, as shown in Fig. 2(a). The dots have uniform size and form multiple grains. We have computed to $t = 10^6$; the dots remain the same size. Without the dipole interaction, i.e., setting $s_1 = 0$, the simulation shows that the dots would have long coarsened into a single large dot. This confirms the refining effect of dipole interaction. Figure 2(b) shows the second layer pattern, which has an average concentration of $\bar{C}_2 = 0.2$ and grows on top of the pattern in Fig. 2(a). We let the second layer evolve from a completely different random initial condition. The dots of the second layer stay at exactly the same positions as those in Fig. 2(b), suggesting the anchoring effect of the first layer. The dot size of the

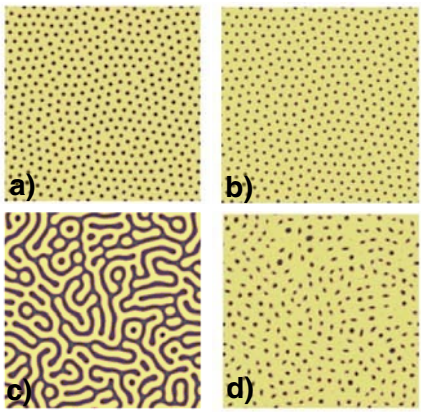

FIG. 2 (color online). Self-assembled patterns with $U = 0$. (a) First layer, $\bar{C}_1 = 0.3$, $t = 3000$. (b) Second layer on top of (a), $\bar{C}_2 = 0.2$, $t = 1000$. (c) First layer, $\bar{C}_1 = 0.5$, $t = 6000$. (d) Second layer on top of (c), $\bar{C}_2 = 0.2$, $t = 2000$.

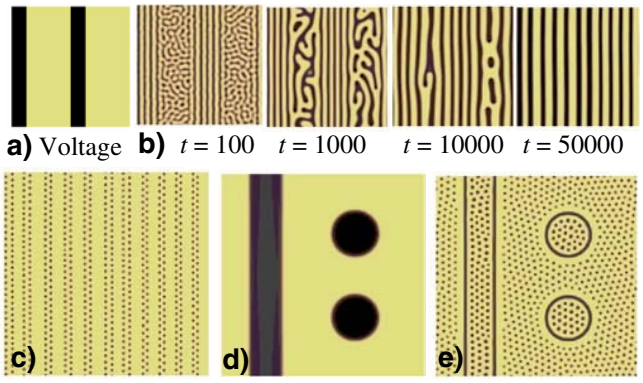

FIG. 3 (color online). Effect of external voltage. (a) Voltage pattern. Dark stripes: $U\varepsilon_s/\eta_1 = 0.1$; other regions: $U = 0$. (b) An evolution sequence. First layer, $\bar{C}_1 = 0.5$. (c) Second layer, $\bar{C}_2 = 0.2$, $t = 1000$. (d) First layer, $\bar{C}_1 = 0.3$, $t = 2000$. (e) Second layer, $\bar{C}_2 = 0.3$, $t = 15\,000$.

second layer is smaller due to lower average concentration. Figure 2(c) shows the first layer pattern for $\bar{C}_1 = 0.5$, which forms a noodle structure. The second layer forms a pattern of dots following the contour of the noodle pattern, as shown in Fig. 2(d). It is not necessary to consider any average concentration greater than 0.5, since this can be easily accommodated by redefining the concentration with the other species. The simulations in Fig. 2 have $\bar{C}_2 < \bar{C}_1$. Our results on $\bar{C}_2 > \bar{C}_1$ demonstrate a similar effect: the second layer follows the pattern of the first layer, but has a larger feature size. The observations suggest that the first layer determines the ordering and lattice spacing, while the second layer determines the feature size. A scaling down of size can be achieved via multilayers. The interesting behavior suggests a potential fabrication method. In addition to self-assembly, the first layer pattern can be defined by embedded electrodes, proximal probe technique, or nanoimprinting.

Now consider the effect of external field. A voltage pattern is defined in Fig. 3(a), dark color for $U\varepsilon_s/\eta_1 = 0.1$ and bright color for $U = 0$. Figure 3(b) shows the evolution of a monolayer with $s_1 = 2$ and $\bar{C}_1 = 0.5$. In contrast to the noodle pattern in Fig. 2(c), an ordered parallel stripe pattern is obtained. After the monolayer evolves to $t = 5 \times 10^4$, we remove the external field, adsorb the second layer, and let it evolve. Figure 3(c) shows the second layer pattern for $s_2 = 6$ and $\bar{C}_2 = 0.2$. The dots form nicely ordered parallel lines along the stripes in the first layer. Another set of simulations is performed to investigate the guiding effect of patterns with larger dimensions. The voltage pattern contains a thick vertical stripe and two disks of $U\varepsilon_s/\eta_1 = 10$, with $U = 0$ in other regions. The first layer, which has $s_1 = 2$ and $\bar{C}_1 = 0.3$, evolves into a pattern shown in Fig. 3(d). Note that the application of a high voltage sweeps off any self-assembled features so that the monolayer replicates the voltage pattern. We then remove the external voltage and let the second layer form and evolve. With $s_2 = 6$ and $\bar{C}_2 = 0.3$, the second layer evolves into a pattern shown in Fig. 3(e). The dots align themselves along the edges of the first layer pattern and form a triangular lattice. It is interesting to note the formation of pairing dark and white lines following the contour of the first layer pattern. Two nearby regions separated by the lines have different preference for the two dipole species. This causes local accumulation and depletion of the two dipoles, resulting in the observed phenomena.

In summary, our work reveals the unique self-assembly behavior of a multilayer of molecules, which may lead to a novel approach for nanopatterning. Experiments have identified electric dipole interaction as the mechanism to cause monolayer pattern formation [13]. Our model captures the physics. The simulations on monolayers have produced patterns consistent with those observed in experiments, such as Fig. 2(a) and 2(c), and predicted the dependence of pattern type on the average concentration. Experiments on multilayers need to be carried out to ascertain the predictions and explore the opportunities.

The authors acknowledge financial support from National Science Foundation Career Award No. DMI-0348375.

*Corresponding author.
Email address: weilu@umich.edu

[1] S. D. Evans, E. Urankar, A. Ulman, and N. Ferris, J. Am. Chem. Soc. **113**, 4121 (1991).
[2] H. M. McConnell, Annu. Rev. Phys. Chem. **42**, 171 (1991); M. Seul and D. Andelman, Science **267**, 476 (1995).
[3] A. J. Dickstein *et al.*, Science **261**, 1012 (1993); J. Richardi, D. Ingert, and M. P. Pileni, Phys. Rev. E **66**, 046306 (2002).
[4] S. J. Stranick *et al.*, J. Phys. Chem. **98**, 7636 (1994); K. Tamada *et al.*, Langmuir **13**, 1558 (1997).
[5] K.-O. Ng and D. Vanderbilt, Phys. Rev. B **52**, 2177 (1995); R. Plass *et al.*, Nature (London) **412**, 875 (2001).
[6] G. L. Kellogg, Surf. Sci. **21**, 1 (1994); J. V. Barth, Surf. Sci. **40**, 75 (2000).
[7] F. Rosei *et al.*, Prog. Surf. Sci. **71**, 95 (2003); A. J. Heinrich *et al.*, Science **298**, 1381 (2002).
[8] S. Y. Chou and L. Zhuang, J. Vac. Sci. Tech. B **17**, 3197 (1999).
[9] Z. Suo, Y. F. Gao, and G. Scoles, J. Appl. Mech. **71**, 24 (2004).
[10] R. K. Iler, J. Colloid Interface Sci. **21**, 569 (1966); W. Q. Jin, A. Toutianoush, and B. Tieke, Langmuir **19**, 2550 (2003); M. F. Durstock *et al.*, J. Appl. Phys. **94**, 3253 (2003).
[11] J. W. Cahn and J. E. Hilliard, J. Chem. Phys. **28**, 258 (1958).
[12] W. Lu and Z. Suo, Phys. Rev. B **65**, 085401 (2002); **65**, 205418 (2002).
[13] F. T. Xu, S. C. Street, and J. A. Barnard, J. Phys. Chem. B **107**, 12762 (2003).